Microphysical and Dynamical Influences on Cirrus Cloud Optical Depth Distributions

J. Kay, M. Baker, and D. Hegg*
University of Washington
Seattle, Washington

**corresponding author, jenkay@u.washington.edu, 206-685-2910*

Introduction

Cirrus cloud inhomogeneity occurs at scales greater than the cirrus radiative smoothing scale (~100 m), but less than typical global climate model resolutions (~300 km). Therefore, calculating cirrus radiative impacts in global climate models requires an optical depth distribution parameterization. Radiative transfer calculations are sensitive to optical depth distribution assumptions (Fu et al. 2000; Carlin et al. 2002). Using raman lidar observations, we quantify cirrus timescales and optical depth distributions at the Atmospheric Radiation Measurement (ARM) Southern Great Plains (SGP) site in Lamont, Oklahoma. We demonstrate the sensitivity of outgoing longwave radiation (OLR) calculations to assumed optical depth distributions and to the temporal resolution of optical depth measurements. Recent work has highlighted the importance of dynamics and nucleation for cirrus evolution (Haag and Karcher 2004; Karcher and Strom 2003). We need to understand the main controls on cirrus optical depth distributions to incorporate cirrus variability into model radiative transfer calculations. With an explicit ice microphysics parcel model, we aim to understand the influence of ice nucleation mechanism and imposed dynamics on cirrus optical depth distributions.

Atmospheric Radiation Measurement Southern Great Plain Raman Lidar Cirrus Observations

Using ~4000 hours of ARM SGP Raman lidar depolarization observations, we investigated cirrus cloud timescales and length scales. We constructed 12-hour ice cloud masks and analyzed cirrus timescales and length scales. The smallest timescales, length scales, and thicknesses dominate cirrus histograms. Covariance analysis revealed few linear relationships between the variables investigated. Average thickness was correlated with standard deviation in thickness (R^2=0.70). Average timescale was correlated with average thickness (R^2=0.64) and standard deviation in thickness (R^2=0.61). Cirrus tended to be thickest and longest between -45 and -55°C, corresponding to a maximum in their abundance.

Cirrus optical depths were estimated using 1-minute lidar backscatter at cloud base and cloud top. Small values dominate a histogram of all cirrus optical depth values; 60% of the optical depths were less

than 0.5. With these retrievals, we investigated cirrus cloud optical depth distributions over 759 3-hour periods. We used a power law fit to relate the mean optical depth and standard deviation in optical depth over 3-hour periods (Figure 1).

Simple calculations of OLR reveal the importance of optical depth distribution assumptions. Using the mean observed optical depth to calculate OLR (the plane parallel homogeneous [PPH] assumption) leads to an average underestimation of OLR by 8 Wm^{-2} when compared to using the observed optical depths (the independent column approximation [ICA]). This OLR PPH bias (OLR ICA – OLR PPH) increases with standard deviation in optical depth (Figure 2). Ten percent of cirrus observations had standard deviations in optical depth greater than 0.7 and OLR PPH biases exceeding 20 Wm^{-2}. Fu et al. (2000) suggested using a gamma distribution to parameterize variability in optical depth. The gamma distribution parameterization, with the mean and standard deviation derived from the lidar observations, decreases the average OLR bias from 8 Wm^{-2} (OLR ICA – OLR PPH) to 1.6 Wm^{-2} (OLR ICA – OLR gamma) (Table 1).

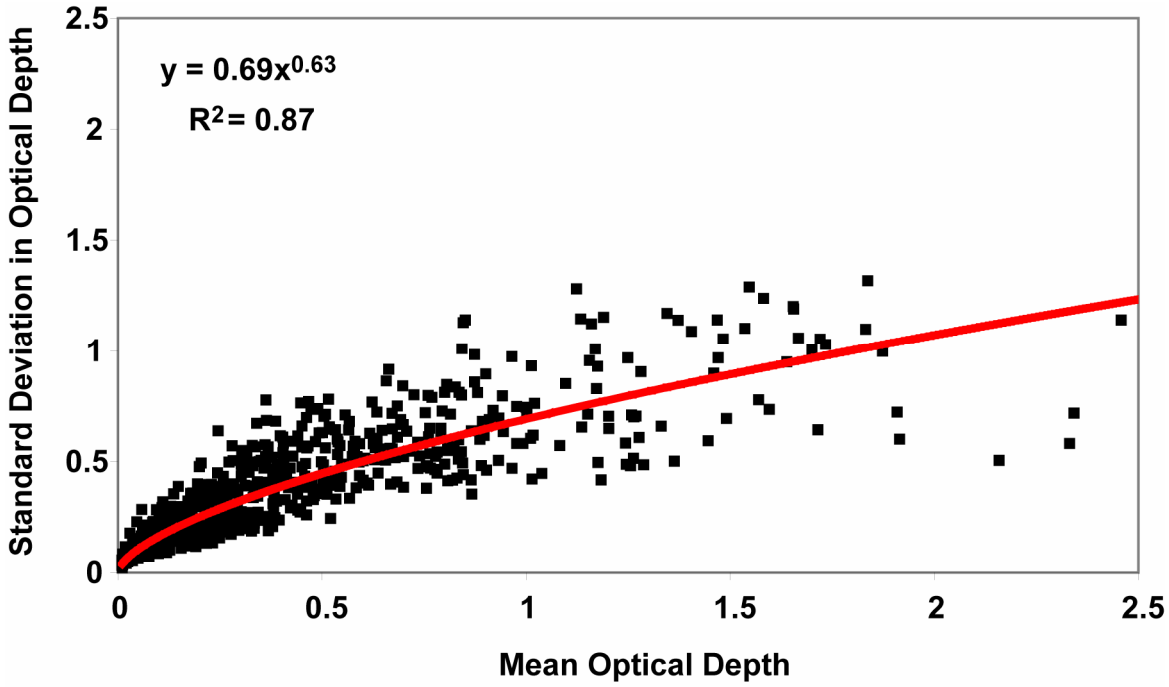

Figure 1. Lamont, Oklahoma, Raman lidar observations of cirrus optical depth variability. A power law relates the observed mean optical depth and standard deviation in optical depth.

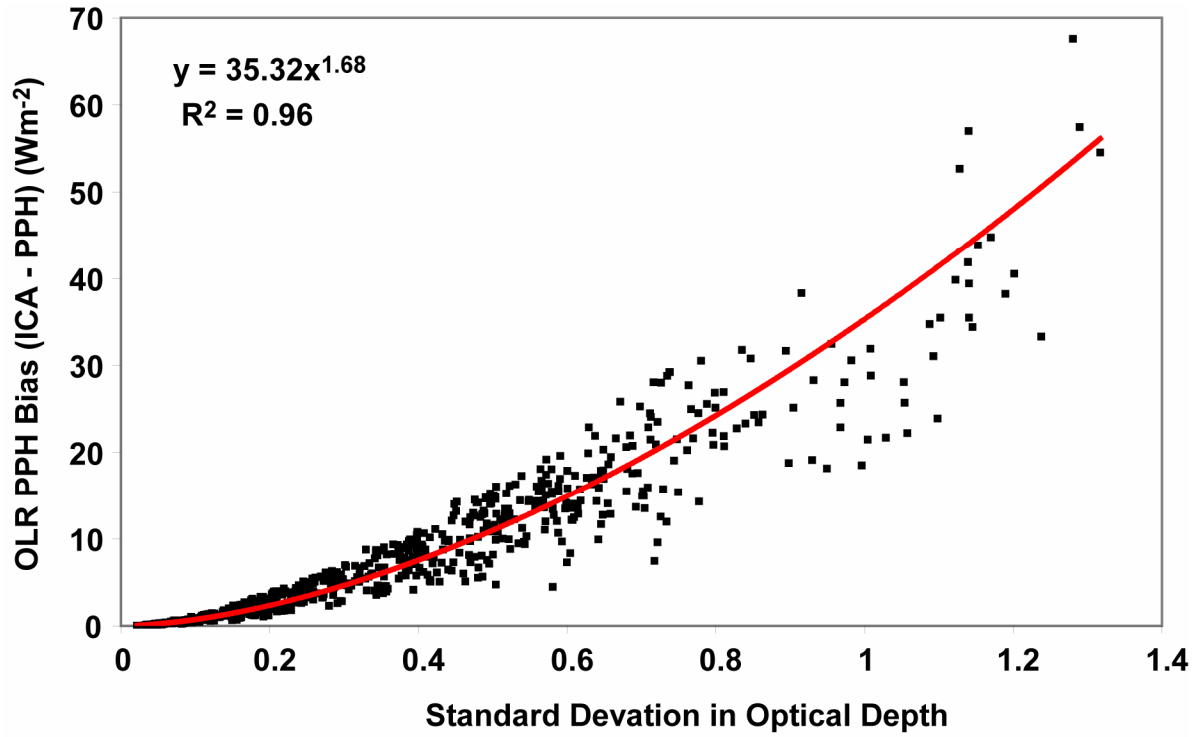

Figure 2. OLR bias from Lamont, Oklahoma, Raman lidar observations. OLR PPH biases increase with observed variability in cirrus optical depth.

Table 1. Biases and absolute deviations from OLR calculated using observed optical depths (ICA approximation)

	PPH (observed mean OD)	Gamma (observed mean OD and observed standard deviation in OD)	Gamma Predicted (observed mean and predicted standard deviation in OD)
Average Bias (ICA - XXX) - Wm^{-2}	8	1.6	1.9
Average Absolute Deviation - Wm^{-2}	9.4 ± 8.1	2.2 ± 2.8	4 ± 4.6

We suggest using the mean observed optical depth to predict the standard deviation in optical depth with the power law fit from Figure 1. This predicted standard deviation in optical depth could then be used for the gamma distribution parameterization (gamma predicted). Although OLR (gamma predicted) has a larger average absolute deviation from OLR (ICA) than OLR (gamma), using the power law fit to predict the standard deviation reduces the average OLR bias from 8 Wm^{-2} (OLR ICA – OLR PPH) to 1.9 Wm^{-2} (OLR ICA – OLR gamma predicted) (Table 1). Thus, using the mean optical depth to predict the standard deviation in optical depth may help alleviate OLR biases that result from cirrus inhomogeneity.

Simple calculations also reveal the importance of the temporal resolution of optical depth observations. The standard deviation in optical depth at 1-minute resolution, 0.36, decreases to 0.29 and 0.22 for 10-minute and 1-hour resolution, respectively. Increased variability in optical depth increases OLR. As a result, the computed ICA OLR also decreases with temporal averaging from 335 Wm^{-2} (1-minute) to 333 Wm^{-2} and 329 Wm^{-2} for 10-minute and 1-hour data, respectively. As expected, the PPH OLR bias is also reduced as the temporal resolution of the optical depth data increases. Therefore, high temporal resolution optical depth observations are necessary to compute accurate OLR and to evaluate potential global climate model biases.

Parcel Model Experiments

Parcel Model Description

We developed an adiabatic parcel model with explicit binned ice microphysics to explore the influence of dynamics and nucleation mechanism on cirrus cloud optical depth distributions. Following Lin et al. (2002), Karcher (2003), and Jacobson (1999), the parcel model calculates the size and concentration of sulfuric acid aerosols, water drops, and ice crystals along prescribed trajectories using specified phase transition criteria and standard diffusion equations. The vapor pressures over ice and supercooled water are specified from a recent compilation by Murphy and Koop (2005). Cloud condensation nuclei (CCN) concentrations are set at 100 cm^{-3} based on aircraft observations in the upper troposphere. Ice particles fall out of the parcel with speeds based on their size and a parcel depth of 100 m. Optical depth calculations assume a cloud depth of 1000 m. Parcel depths are smaller than cloud depths to account for multiple cloud layers. Parcel evolution is sensitive to the parcel depth, but cloud depth is simply a scalar required for optical depth calculations.

Traditionally, homogeneous and heterogeneous nucleation have been distinguished by the differing number concentrations of aerosols available for freezing (i.e., CCN versus ice nuclei [IN] concentrations), and the differing temperature and relative humidity $(RH)_{ice}$ freezing thresholds. Our parcel model uses homogeneous nucleation rates derived as functions of aerosol water activity or ambient RH (Koop et al. 2000). Given our limited knowledge about heterogeneous nucleation, we investigate the role of IN concentration and IN activation. IN concentrations are set following atmospheric observations from Storm Peak, Colorado (generally <0.03 cm^{-3} from [DeMott et al. 2004]), and SUCCESS flights (maximum 0.1 cm^{-3} from [Rogers et al. 1998]). IN are activated as an exponential function of RH_{ice} (Meyers et al. 1992) or as a step function at a specified RH_{ice} (130%) ("Step Activation"). Developed for higher temperatures and lower RH_{ice}, the Meyers IN parameterization exceeds observed IN concentrations at high RH with respect to ice (RH_{ice}). Therefore, we also include a modified Meyers activation where the maximum IN concentration is set at 130% RH_{ice} (0.026 cm^{-3}) (Meyers et al. 1992).

To simulate dynamic variability, we use constant updrafts, idealized sinusoidally varying vertical velocity velocities and kinematic trajectories derived from a mesoscale numerical weather model (MM5). Idealized sinusoidally varying vertical velocity trajectories are described using a constant updraft (w_o), and a superimposed wave amplitude (A) and period (P).

Parcel Model Experiment #1: Homogeneous Nucleation Only With Superimposed Sine Waves

In the first parcel model experiment, we explored the role of superimposed waves on cirrus evolution with only homogeneous nucleation. We found amplitudes of at least 0.1 m/second and 100-second periods were necessary to significantly change (>10%) the maximum IWC and maximum number concentration of ice crystals (N_{ice}) of lifted parcels. Figures 3a and 3b show the vertical velocity and displacement trajectories and resulting evolution of N_{ice}, optical depth and IWC for mesoscale (P=1000 seconds, ~30 km wavelengths) and synoptic scale (P=10,000 seconds, ~300 km wavelengths) superimposed waves. Large amplitude mesoscale waves increased maximum N_{ice}, lengthened cirrus lifetimes, and imprinted wave dynamics on the optical depth evolution. These mesoscale waves increased the fallout timescales and led to broader optical depth distributions. Superimposed synoptic waves, with periods longer than the average cirrus fallout timescale, resulted in the largest parcel IWC and IWC lost. Although large optical depths were generated, the smaller N_{ice}, significant particle growth and resulting fallout led to shorter cloud lifetimes and narrower optical depth distributions.

Parcel Model Experiment #2: Homogeneous and Heterogeneous Nucleation with Superimposed Waves

In the second parcel model experiment, we explored the role of waves on cirrus evolution with both homogeneous and heterogeneous nucleation. Figure 3c shows the resulting N_{ice}, optical depth and optical depth distributions for a constant updraft and high amplitude mesoscale superimposed waves. Just like parcel model experiment #1, the optical depth distributions for the mesoscale waves were all broader than for the constant updraft.

For all runs with IN concentrations less than the maximum observed IN concentrations (0.1 cm^{-3} – [Rogers et al. 1998]), homogeneous nucleation was not inhibited by heterogeneous nucleation. As a result of continued lifting and fallout, homogeneous nucleation occurred after an initial heterogeneous nucleation event. With larger IN concentrations, there were greater delays between the initial heterogeneous nucleation event and subsequent homogeneous nucleation events. For the constant updraft (left panel of Figure 3c), ice crystals formed by heterogeneous nucleation events at minute 45 for all step activation IN parameterizations. After these initial ice crystals fall out, homogeneous nucleation events occurred at minute 70 for step activation IN=0.003 cm^{-3}, minute 90 for step activation IN=0.026 cm^{-3} and minute 110 for step activation IN=0.1 cm^{-3}. For the mesoscale waves (right panel of Figure 3c), early heterogeneous nucleation also delayed homogeneous nucleation. For high IN concentrations (step activation IN=0.1 cm^{-3}), the delayed homogeneous nucleation event at minute 85 had greater N_{ice}.

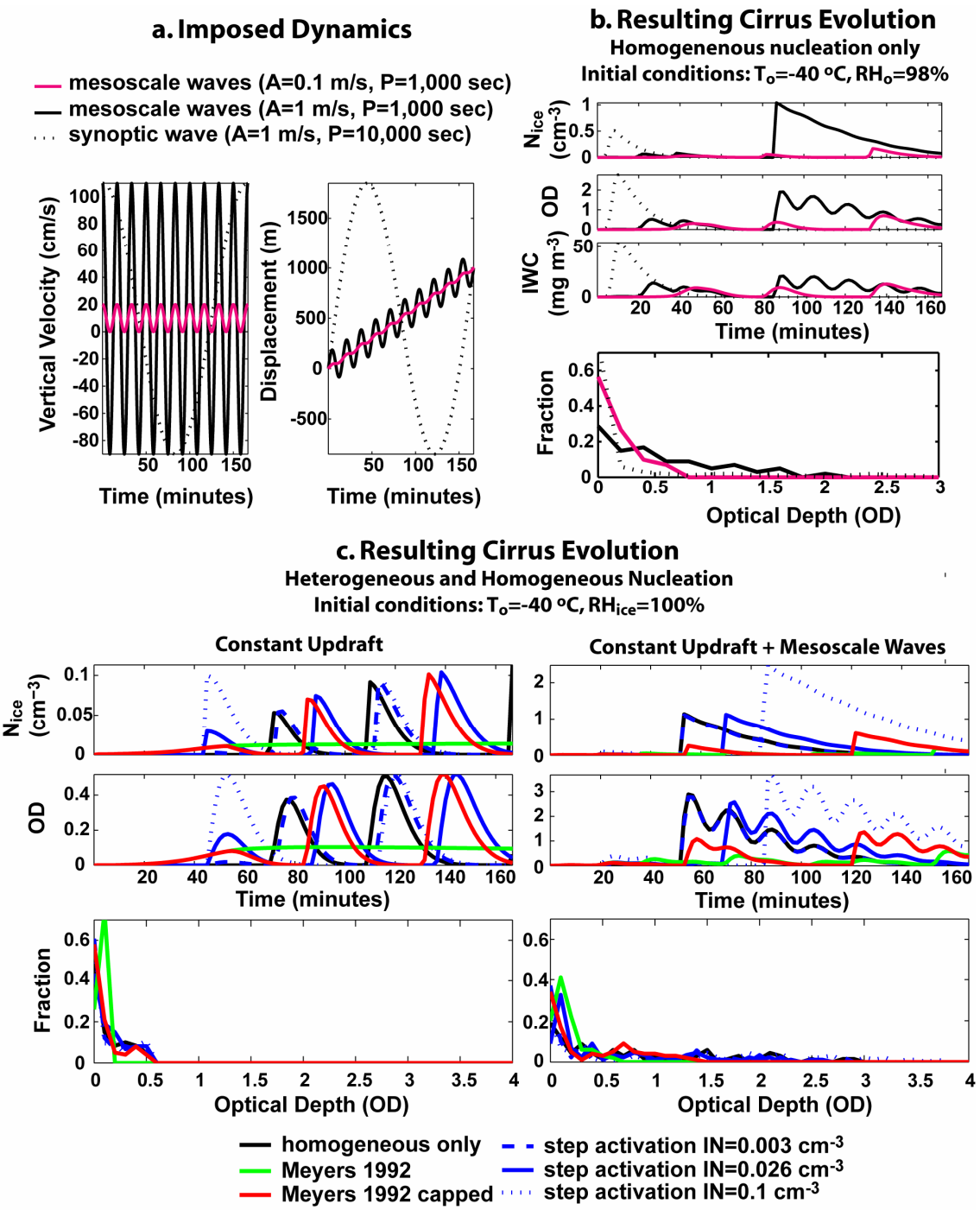

Figure 3. Effect of superimposed waves on cirrus evolution. a) Imposed dynamics. Vertical velocity (w) = w_o+Asin(2π/Pt). w_o = 10 cm/sec for all trajectories. b) Resulting cirrus evolution with homogeneous nucleation. High-amplitude mesoscale waves imprint dynamics on cirrus evolution and broaden optical depth distributions. c) Resulting cirrus evolution with homogeneous and heterogeneous nucleation. Superimposed mesoscale waves (A=1 m/sec, P=1000 sec) broaden optical depth distributions Heterogeneous nucleation shifts and changes the magnitude of subsequent homogeneous nucleation events.

Comparing exponential (Meyers et al. 1992) and step (step activation IN=0.026 cm^{-3}) activation allows us to evaluate the role of IN parameterization independent of IN limiting concentration. With a constant updraft, exponential IN activation resulted in timing changes for heterogeneous and homogeneous nucleation events, but very similar optical depth distributions when compared to step IN activation (left panel, Figure 3c). With superimposed mesoscale waves, exponential IN activation suppressed homogeneous nucleation, resulting in a narrower optical depth distribution than step IN activation (right panel, Figure 3c).

The Meyers 1992 IN activation exceeded the maximum observed IN concentrations (0.1 cm^{-3}) for the constant updraft trajectory (0.17 cm^{-3}) and superimposed mesoscale waves trajectory (0.42 cm^{-3}). The exponential activation also allowed the Meyers runs to achieve a steady state between fallout and continued IN activation from the lift-generated ice supersaturation. As a result, the Meyers 1992 parameterization was able to suppress homogeneous nucleation. This unlimited source of IN at high supersaturations is not supported by atmospheric observations (Rogers et al. 1998; DeMott et al. 2004).

Parcel Model Experiment #3: MM5 Trajectories

On April 19-20, 2001, cirrus clouds formed in the lee of the Southern Rockies and were advected by a broad 300-mb ridge to the ARM SGP site. The Raman lidar observations revealed cirrus with broad optical depth distributions and maximum optical depths above 3. To estimate the vertical velocity trajectories at cirrus altitudes, we ran the PSU/National Center for Atmospheric Research mesoscale model (MM5) from 12 Universal Time Coordinates (UTC) April 18 to 00 UTC April 20 with two domain set-ups: 1) single domain with 36-km grid cell resolution 2) three nested interacting domains with 36-km, 12-km and 4-km grid cell resolutions. A planar view of the trajectories ending at ARM SGP at 00 UTC on April 20, 2001, is shown in Figure 4.

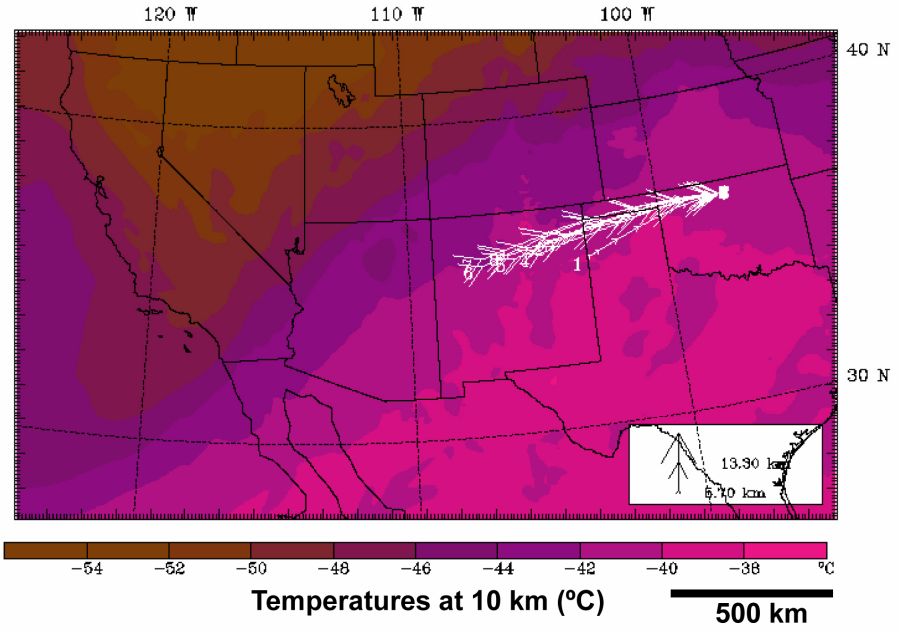

Figure 4. MM5 trajectories ending at multiple heights on April 20, 2001 (00 UTC).

Figure 5 (left panel) shows the vertical velocity and displacement for the trajectory ending 12 km above the ARM SGP site. Not surprisingly, the amplitude of vertical velocities along trajectories increased with MM5 grid cell resolution. The 36-km single domain had lower maximum vertical velocities (<10 cm/sec) than any of the nested domains. The 12- and 4-km nested domains had mesoscale vertical velocity variability (30-45 km wavelength) with amplitudes exceeding 1 m/s. In these high resolution domains, non-hydrostatic orographic waves were induced as the trajectories traveled over the Southern Rocky Mountains. Two-way nesting allowed communication of the orographic waves to the nested 36-km domain trajectory but not the single 36-km domain trajectory.

Parcel model runs along the MM5 trajectories reveal the importance of the domain dynamics to cirrus formation and evolution (Figure 5 right panel). For this experiment, we used only homogeneous nucleation. For initial conditions, we set the initial RH_{ice} to 100% and used the initial temperature and heights from MM5. Along the 36-km domain trajectory, the RH_{ice} remained below the homogeneous nucleation thresholds, and no ice clouds formed. For the nested domains, larger vertical velocities and greater vertical displacement resulted in cirrus cloud formation. Cirrus optical depths were greatest with the 4 km domain trajectory, which had the largest vertical velocity at ice formation. Along the nested domain trajectories, cirrus persisted for many hours and had MM5 dynamics imprinted on the optical depth evolution. The large vertical velocities and cold temperatures at 12 km enhanced homogeneous nucleation rates, resulting in longer cirrus lifetimes and broader cirrus optical depth distributions.

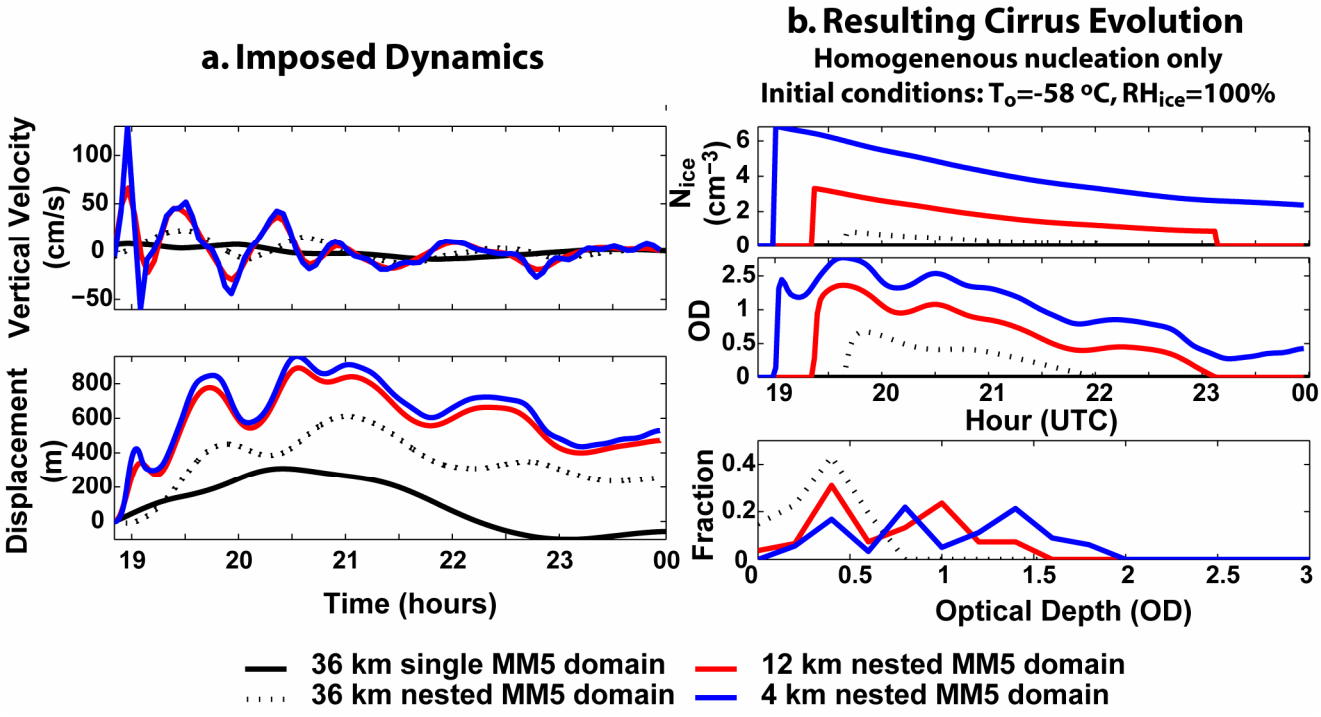

Figure 5. Dynamics and cirrus evolution for MM5 trajectory ending at 00 UTC April 20, 2001 12 km above Lamont, Oklahoma. a) Imposed dynamics. Vertical velocity trajectories depend on MM5 resolution and nesting. b) Resulting cirrus evolution. Cold temperatures and large vertical velocity at ice formation result in persistent cirrus with broad optical depth distributions.

Summary and Future Work

Short timescales (< 10 minutes) and small optical depths dominate cirrus lidar observations. Computed OLR is sensitive to optical depth distribution, especially when optical depth distributions are broad. Without understanding observed optical depth distributions, it will be difficult to incorporate cirrus variability into climate models. Parcel model experiments with a constant parcel depth of 100 m show that mesoscale waves and cold temperatures broaden cirrus optical depth distributions. With atmospherically relevant concentrations and idealized trajectories, heterogeneous nucleation does not inhibit homogeneous nucleation, but it can shift the timing and sometimes the magnitude of homogeneous nucleation. For a ridge case study on April 19, 2001, MM5 predicted that trajectories have orographic mesoscale waves that broaden computed optical depth distributions. We also find the resolution of MM5 simulations affects calculated cirrus optical depth distributions. We plan to continue parcel model experiments along idealized and MM5 trajectories to understand how nucleation rate, temperature, parcel depth, and vertical velocity history affect cirrus optical depth distributions. This work will help improve representation of cirrus optical depth distributions and radiative impacts in models.

Acknowledgments

We thank Dave Turner, Pacific Northwest National Laboratory, for providing lidar optical depth retrievals and Tom Ackerman, Qiang Fu, Dave Turner, and Jennifer Comstock for fruitful research discussions.

References

Carlin, B, Q Fu, U Lohmann, G Mace, K Sassen, and J Comstock. 2002. "High-cloud horizontal inhomogeneity and solar albedo bias." *Journal of Climate* 15(17):2321-2339.

DeMott, PJ, DJ Cziczo, AJ Prenni, DM Murphy, SM Kreidenweis, DS Thomson, R Borys, and DC Rogers. 2003. "Measurements of the concentration and composition of nuclei for cirrus formation." *Proceedings of the National Academy of Sciences of the United States of America* 100(25):14655-14660.

Fu, Q, B Carlin, and G Mace. 2000. "Cirrus horizontal inhomogeneity and OLR bias." *Geophysical Research Letters* 27(20):3341-3344.

Haag, W, and B Karcher. 2004. "The impact of aerosols and gravity waves on cirrus clouds at mid-latitudes." *Journal of Geophysical Research* 109(D12):D12202.

Jacobson, MZ. 1999. "Fundamentals of Atmospheric Modeling." Cambridge University Press.

Karcher, B. 2003. "Simulating gas-aerosol-cirrus interactions: Process-oriented microphysical model and applications." *Atmospheric Chemistry and Physics* 3:1645-1664.

Karcher, B, and J Strom. 2003. "The roles of dynamical variability and aerosols in cirrus cloud formation." *Atmospheric Chemistry and Physics* 3:823-838.

Koop, T, B Luo, A Tslas, and T Peter. 2000. "Water activity as the determinant for homogeneous ice nucleation in aqueous solutions." *Nature* 406:611-614.

Lin, R, DO'C Starr, P DeMott, R Cotton, K Sassen, E Jensen, B Karcher, and X Liu. 2002. "Cirrus parcel model comparison project. Phase 1: The critical components to simulate cirrus initiation explicitly." Journal of the Atmospheric Sciences 59(15):2305-2329, 59:15.

Meyers, MP, PJ DeMott, and WR Cotton. 1992. "New primary ice-nucleation parameterization in an explicit cloud model." *Journal of Applied Meteorology* 31(7):708-721.

Murphy, DM, and T Koop. 2005. "Review of the vapor presser of ice and supercooled water for atmospheric applications." *Quarterly Journal of the Royal Meteorological Society*, in press.

Rogers, DC, PJ DeMott, SM Kredenweis, and Y Chen. 1998. "Measurements of ice nucleating aerosols during SUCCESS." *Geophysical Research Letters* 25(9):1383-1386.